Chapter 6
PELDOR in Peptide Research

Abstract The measurement of distances within and between peptides is an important application of PELDOR or DEER spectroscopy in biology. Individual measurements have been made on many proteins and provide distance information that have been vital for understanding the properties of those proteins. However, the most thoroughly studied peptides belong to the class of peptaibols.

Peptides are chains of amino acids linked by amide bonds. They are the major component of proteins and enzymes. The folding of peptides into three-dimensional structures and changes in the conformations of those structures play vital roles in all living organisms. The exact sequence of the different amino acids making up a protein have a profound influence on both structure and biological function. The measurement of distances within and between peptides is an important application of PELDOR in biology. Individual measurements have been made on many proteins and provide distance information that have been vital for understanding the properties of those proteins. However, the class of peptides most-thoroughly studied by PELDOR are the peptaibols.

The site-directed spin labeling of peptides allows PELDOR methods to provide quite detailed structural information on peptides in solution, in aggregates and absorbed on surfaces. The distance distribution spectra can reveal structural heterogeneity and can measure the shifts in population. PELDOR also retains the high specificity and selectivity of EPR for the spin-labeled peptides without the restrictions on optical properties or crystallinity required by other structural techniques.

6.1 Spin-Labeled Peptaibols

The peptaibols are members of a class of largely hydrophobic, membrane-active, linear peptides up to 21 α-amino acids in length and typically having antibiotic activity [1–11]. They often contain the unusual amino acid α-aminoisobutyric acid

Y. D. Tsvetkov et al., *Pulsed Electron–Electron Double Resonance*,
https://doi.org/10.1007/978-3-030-05372-7_6

(Aib), Table 6.1. Unlike the common amino acids, the C^{α} of Aib has four chemical bonds to heavy atoms and none to hydrogen. As a result, the Aib residue is stiffer than other amino acids and strongly foldameric or helicogenic [12, 13], so that peptaibols strongly prefer helical structures in artificial bilayers and in natural membranes where they are bioactive. Peptaibols typically have an N-terminal acyl group, either acetyl or a long chain acyl, and a C-terminal 1,2-amino alcohol which eliminates the terminal positive and negative charges from the backbone. In Nature, most peptaibols exhibit microheterogeneity, i.e., they are a mixture of very similar peptides with numerous conservative changes in their amino acid sequence.

Knowledge about the 3D-structure and properties of peptaibols and their aggregates is necessary for the design of efficient antibiotics based on peptaibols. PELDOR studies have revealed several structural peculiarities, including aggregation of peptaibols into a range of different structures in membrane-mimicking solvents, in lipid model systems, as well as in bacterial cells. Structural details are obtained from the dipole-dipole interactions between spin labels introduced at specific sites in the peptaibol. The TOAC nitroxyl spin label, **4-22**, [14] is typically used for PELDOR studies of peptaibols, Table 6.1. TOAC is covalently and rigidly embedded in the peptide sequence, replacing an Aib and is equally helicogenic. TOAC eliminates the flexible side-chain linker to the nitroxyl group that is inherent in every other amino acid spin label. Consequently, TOAC produces very accurate measurements of the distance between spins, although TOAC's six-membered ring may adopt at least two conformations [15–17].

Formation of pores in biological membranes eventually generates cell leakage and is generally believed to be a basis for the antibiotic activity of membrane-active peptides. Peptaibols are intriguing because many of them can be activated by a membrane voltage [1, 2, 4, 9–11, 18, 19] even though they are electrically neutral. But their ability to cause membrane leakage in the absence of a membrane voltage is even more challenging to explain.

PELDOR provides extremely useful information on the overall 3D-structure and self-association modes of biomolecules in membranes [20]. Other spectroscopic techniques, such as fluorescence, and in particular, fluorescence resonance energy transfer, FRET, can provide complementary information to confirm and further refine the picture provided by PELDOR data.

6.1.1 Secondary Structure

A variety of site-directed mono- and double-labeled peptaibols with various main-chain lengths, Table 6.1, have been studied. The PELDOR experiments discussed here were made with spin-labeled peptaibols prepared by chemical synthesis. A CW EPR approach to correlate peptide conformation with distance between two TOAC labels has been suggested, but seems limited to short distances <1.5 nm [15–17]. PELDOR experiments were performed at X-band on the homemade ICKC or commercial E580 pulsed EPR spectrometers using 3p- or

Table 6.1 Amino acid sequences of peptaibols investigated by PELDOR spectroscopy, bold characters indicate **Aib** residues potentially replaced by TOAC spin label **4-22** in the labeled analogs, with labeled sites indicated by superscripts

Abbreviation	Name sequence[a]
O-Tri	Trichogin GA IV[c] Oct·**Aib^{1}**·Gly·Leu·**Aib^{4}**·Gly·Gly·Leu·**Aib^{8}**·Gly·Ile·Leu·OMe
F-Tri	Trichogin GA IV[b] Fmoc·**Aib^{1}**·Gly·Leu·**Aib^{4}**·Gly·Gly·Leu·**Aib^{8}**·Gly·Ile·Leu·OMe
Tyl	Tylopeptin B[b] Ac·Trp·Ala·**Aib^{3}**·Aib·Ala·Gln·Ala·**Aib^{8}**·Ser·Aib·Ala·Leu·**Aib^{13}**·Gln·Lol
Hep	Heptaibin Ac·Phe·**Aib^{2}**·Aib·Aib·Val·Gly·Leu·Aib·Aib·Hyp·Gln·Aib·Hyp·**Aib^{14}**·Phl
Amp	Ampullosporin A[b] Ac·Trp·Ala·**Aib^{3}**·Aib·Leu·Aib·Gln·Aib·Aib·Aib·Gln·Leu·**Aib^{13}**·Gln·Leu·OMe
Zrv	Zervamicin IIa[b] **T^{N}**·Trp·Ile·Gln·Aib·Ile·Thr·Aib·Leu·Aib·Hyp·Gln·Aib·Hyp·Aib·Pro·**T^{C}**
Alm	Alamethicin F50/5[b] Ac·**Aib^{1}**·Pro·Aib·Ala·Aib·Ala·Glu(OMe)·**Aib^{8}**·Val·Aib·Gly·Leu·Aib·Pro·Val·**Aib^{16}**· Aib·Glu(OMe)·-Glu(OMe)·-PheOMe·Ac
D-Tri	Trichogin GA dimer[b] Ac·**Aib^{1}**·Gly·Leu·Aib·Gly·Gly·Leu·Aib·Glu·Ile·Leu·Aib·Gly·Leu·Aib·Gly·Gly·Leu·**Aib^{19}**· Gly·Ile·Leu·OMe

[a]Other abbreviations used: Oct, 1-octanoyl; OMe, methoxy; Fmoc, 9-fluorenyimethoxycarbonyl; Ac, acetyl; Lol, leucinol; Hyp, (4R)-hydroxy Pro; Phol, phenylalaninol; Glu(OMe), γ-methyl Glu
[b]Analog

4pPELDOR. Solid glassy samples in organic solvents were measured at cryogenic temperatures, usually 77 K. Additional experimental details are given in the text or in Chap. 2.

In almost all cases, one or two Aib residues [12, 13] were replaced by equally helicogenic TOAC spin labels [14], Table 6.1. The exceptions include two zervamicin analogs labeled with the TEMPO **4-19** derivatives **T^{N}** and **T^{C}** [21, 22], Table 6.1, attached through an amine or carbonyl group at their N- or C-terminus, respectively.

In polar solvents, such as alcohols, peptaibols are monomeric, but usually self-aggregate in less polar solvents. This offers an opportunity to study their 3D-structure and supramolecular aggregation independently. Information about the secondary structure of peptaibols in the monomeric state as well as in the aggregated state can be obtained from PELDOR spectroscopy of doubly spin-labeled peptides. The global quaternary structure of the aggregates can be obtained from mono spin-labeled peptides.

The determination of the peptide conformation by PELDOR uses doubly-labeled peptide dissolved as monomers in a glassy polar solution. The modulation of the PELDOR signal provides a distance distribution spectrum $F(r)$ between the two labels as described in Sects. 1.2 and 1.3. The peptide conformation is determined

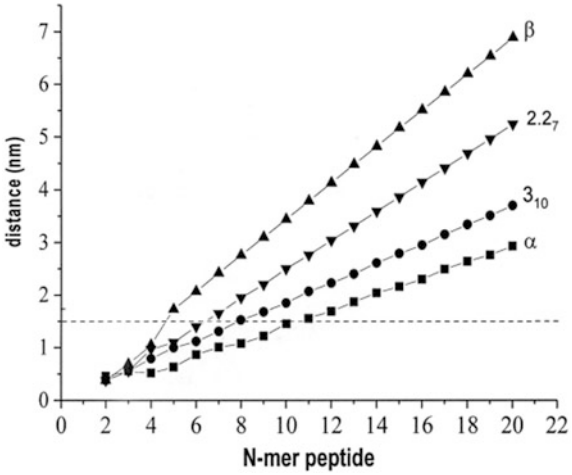

Fig. 6.1 Calculated distances between C^{α} atoms of the terminal residues of *N*-mer peptides for standard α-, 3_{10}-, and 2.2_7-helix and β-sheet conformations: PELDOR measurements of distances are reliable with an accuracy of ±0.03 nm between about 1.5 (*dashed line*) and 8 nm; qualitative information for shorter distances can be obtained by CW EPR spectroscopy. Reproduced from Milov et al. [22] with permission of John Wiley and Sons, copyright 2007

by comparing the measured $F(r)$ with calculated distances between label sites for models of the possible peptide conformations.

The conformational space of peptides is restricted to a range of ϕ and ψ backbone torsion angles, e.g., on the Ramachandran plot, that define α-, 3_{10}-, and 2.2_7-helices, and β-sheet conformations [12, 13, 23–27]. Several helices are possible, each having different patterns of H-bonding between C=O and N–H groups of the peptide backbone. In proteins, 3_{10}-helices have been proposed as kinetic intermediates in the folding and unfolding of long α-helices [28, 29]. In heptapeptides, these two helix conformations occur with roughly equally probability [12, 13, 23, 27]. Many of the very short, Aib-rich peptides prefer the 3_{10}-helix.

The H-bonding patterns produce different lengths for a given peptide, with length increasing in the order α- < 3_{10}- < 2.2_7-helix < β-sheet. This link between conformation and length is the crucial relation that allows peptide conformation to be determined by PELDOR. Distances between terminal residues are calculated for peptides of increasing length in different conformations in Fig. 6.1 [22].

Trichogin GA IV

CW EPR spectra of doubly spin-labeled trichogin GA IV **O-Tri** and **F-Tri** have a weak half-field transition near $g = 4.0$ in frozen glassy solutions [17]. This formally 'forbidden' transition becomes partially allowed by the dipolar interactions between spin labels at fairly short distances. Based on the intensity of this line, the conformation of this short lipopeptide with eleven amino acid residues was assigned as a mixed α/3_{10}-helix, as found by X-ray diffraction in crystals of trichogin GA IV

and **O-Tri**^{4,8}, Table 6.1 [7, 8]. However, PELDOR data reveals that the conformation of **O-Tri**^{1,8} depends on the nature of its solvent, Table 6.2 [30–32]. In frozen methanol (MeOH) or in chloroform/dimethylsulfoxide ($CHCl_3$/DMSO) (7:3) the experimental interspin distance, r = 1.97 nm, corresponds to a mixed $2.2_7/3_{10}$-helix, while in 2,2,2-trifluoroethanol (TFE), the distance is shorter, r = 1.53 nm, corresponding to a pure 3_{10}-helix [31]. Although the ribbon-like 2.2_7-helix is seldom seen [27] and it is difficult to discriminate between 2.2_7- and 3_{10}-helices shorter than r = 1.70 nm, Fig. 6.1, both results are supported by CW EPR experiments [15].

PELDOR can determine the conformation of peptides even in the aggregated state. The double spin-labeled peptide must be diluted with its unlabeled counterpart to minimize intermolecular dipole-dipole interactions. This strategy showed that **O-Tri**^{1,8} has a 3_{10}-helical conformation in the aggregated state [32]. Short peptaibols, such as trichogin, have conformational flexibility, and their structure depends on temperature and on the nature and organization of their surroundings, e.g., glassy state, crystalline state, etc.

Tylopeptin B, Heptaibin, and Ampullosporin A

The distance distribution spectrum $F(r)$ of **Tyl**^{3,13}, Table 6.1, a 14-amino acid analog of tylopeptin B, has a single Gaussian-shaped peak, $r_{max} = 1.76$ nm, Fig. 6.2a and Table 6.2 [35, 39]. The main part of the spectrum for **Hep**^{2,14}, a 14-amino acid residue analog of heptaibin also has a Gaussian shape, but it is broader and shifted to longer intramolecular distances, $r_{max} = 2.3$ nm, Fig. 6.2a and Table 6.2 [35, 39]. These results indicate that **Hep**^{2,14} has a 3_{10}-helical conformation, while **Tyl**^{3,13} seems to adopt a largely α-helical conformation. These two peptaibols have the same number of amino acids, although they adopt different conformations. One significant difference between these two peptaibols is that only the heptaibin analog contains the dipeptide sequence Aib-Hyp which particularly favors the more elongated 3_{10}-helix.

The spin-labeled **Amp**^{3,13} analog of ampullosporin A is another 14-amino acid residue peptaibol, which was studied both by CW EPR and PELDOR [40] in glassy MeOH at 77 K. From PELDOR experiments, the distance spectrum exhibits a main, Gaussian line with a peak at $r_{max} = 1.73$ nm, Table 6.2. Similar results were found from CW EPR analysis and by using convolution/deconvolution methods [41, 42]. The interspin distance of 1.73 nm suggests that **Amp**^{3,13} adopts a mainly α-helical structure, in agreement with CD and fluorescence data in the same paper [40].

Zervamicin II A

Zervamicin II A is a peptaibol with an additional amino acid residue, for a total of 15 residues. X-Ray diffraction and NMR analysis indicated that it folds in a mixed conformation with an α-helix at the N-terminus and a 3_{10}-helix at the C-terminus [28, 43, 44]. The **T**$^{\mathbf{N}}$**-Zrv-T**$^{\mathbf{C}}$ analog with TEMPO spin labels attached at each end, was studied by PELDOR in frozen solutions of MeOH, MeOH/toluene, and MeOH/$CHCl_3$ [21, 22]. In MeOH, the main maximum of the distribution function lies at a distance of ~3.2 nm, Table 6.2. This distance appears to depend only slightly on

Table 6.2 Dependence of conformation[a] on solvent polarity and oligomeric number for double spin-labeled peptaibol analogs of different length [33]

Peptaibol analog	Solvent	Oligomeric number (N)	Distance, r (nm)	Δ (nm)	Helix type	References
O-Tri^{1,8}	$CHCl_3$/toluene 7:3	4	1.57		3_{10}	[32]
O-Tri^{1,8}	$CHCl_3$/DMSO, MeOH	1	1.97		2.2_7/ 3^b_{10}	[31]
O-Tri^{1,8}	TFE	1	1.53		3_{10}	[31]
Tyl^{3,13}	MeOH/ethanol 95:5	2	1.76	0.07	α	[34, 35]
Hep^{2,14}	MeOH/ethanol 95:5	2	2.30	0.07	3_{10}	[34, 35]
Amp^{3,13}	MeOH	1	1.73	0.05	α	[35]
T^N-Zrv-T^C	MeOH	2	3.20	0.3[c]	α/3^b_{10}	[21, 22]
Alm^{1,16}	MeOH	8	2.1	0.3[c]	α	[36]
Alm^{1,16}	MeOH/toluene 1:4	8	2.1	0.3[c]	α	[36]
D-Tri^{1,19}	MeOH	1	2.8/3.2	2	α, 3^b_{10}	[37, 38]
D-Tri^{1,19}	MeOH/toluene, $CHCl_3$/toluene	2	2.8	0.3	α	[37, 38]

[a]Determined for the segment $Aib^i - Aib^j$ from the $TOAC^i$ to $TOAC^j$ distances at 77 K
[b]The notations "$2.2_7/3_{10}$" and "α/3_{10}" indicate mixed conformations within *each* molecule, while "α, 3_{10}" is used for a mixture of molecules with *different* conformations
[c]Asymmetric distance distributions due to the slightly increased flexibility of the TEMPO labels $\mathbf{T^C}$ and $\mathbf{T^N}$

the solvent composition, but the distribution function narrows after addition of either $CHCl_3$ or toluene to the MeOH. This effect was rationalized in terms of decreased mobility at both termini. Molecular dynamics simulations showed that the dominant PELDOR distance agrees well with the mixed α/3_{10}-helix previously determined by NMR. However, when toluene was added to the MeOH solution to further increase the hydrophobicity of the solvent, a minor fraction (7–8%) appears with a distance of 4.2 nm. Most likely, this conformation corresponds to the more elongated 2.2_7-helix for this membrane-active peptide.

Alamethicin F50/5

The double spin-labeled **Alm^{1,16}**, Table 6.1, is an analog of the long, 19-amino acid peptaibol alamethicin F50/5 [45]. It was investigated in frozen solutions of MeOH and MeOH/toluene (1:4), Table 6.2 [36]. The $r_{max} \sim 2.1$ nm distance found in both solvents was in excellent agreement with average distances calculated from a set of five models based on the almost-completely α-helical crystal structures [5, 46]. The distance between labels corresponds to an α-helix, at least for the segment between the labels at residues 1 and 16. Compared to trichogen which has different conformations in different solvents, alamethicin has a remarkably stable conformation. In particular, its conformation remains constant as polarity changes from MeOH to MeOH/toluene.

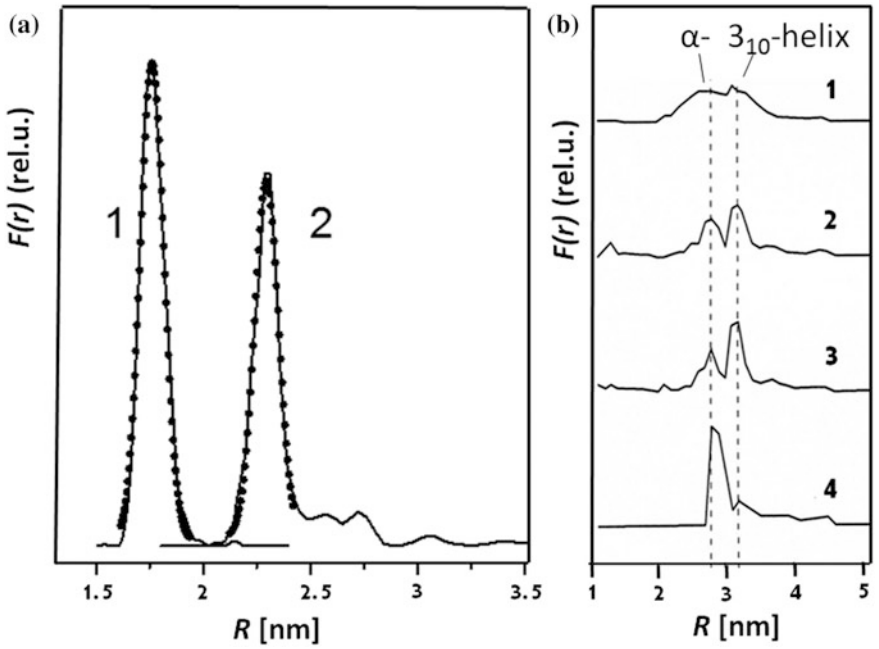

Fig. 6.2 Conformation and environment dependencies: **a** intramolecular distance distributions between spins in the doubly spin-labeled peptaibol analogs *1* **Tyl**[3,13] and *2* **Hep**[2,14] agree with a 3_{10}- and an α-helix conformation, respectively, see Fig. 6.1; **b** changes in the distance distribution function $F(r)$ of **D-Tri**[1,19] with solvent polarity: *1* MeOH; *2* MeOH/toluene 10%; *3* MeOH/toluene 20% MeOH; and *4* chloroform/ toluene. Reproduced from Milov et al. [39] with permission of Springer, copyright 2013 and from Milov et al. [33]

Covalent Dimer of Trichogin GA IV

The longest peptaibol examined by PELDOR is a 22-amino acid, covalently-linked dimer of Trichogin GA IV, designed and synthesized explicitly for PELDOR to test models of aggregation. The distance distribution functions obtained for the doubly spin-labeled **D-Tri**[1,19], Table 6.1, in MeOH/toluene mixtures, Fig. 6.2b, reveals the effect of solvent on self-aggregation and the concomitant alteration of secondary structure [37, 38]. In pure MeOH, the PELDOR time trace $V(T)$ has weak oscillations and $F(r)$ has a poorly-resolved doublet nearly 2 nm wide, Table 6.2. Addition of toluene increases the oscillation amplitude and $F(r)$ exhibits two distinct maxima at $r_{max} = 2.8$ and 3.2 nm corresponding to α-helix and 3_{10}-helix conformations, respectively, Fig. 6.2b. In pure toluene, $V(T)$ is strongly modulated and the main $F(r)$ peak corresponds to α-helical, aggregated molecules.

6.1.2 *Quaternary Structures in Frozen Solutions*

Spin-labeled peptaibols aggregate in solvent mixtures with low polarity. Their quaternary structures, or arrangement of peptides within an aggregate, are obtained by PELDOR spectroscopy from dipolar interactions between labels in different peptides.

Trichogin GA IV

The transition from polar to nonpolar solvents changes the conformation of trichogins and causes aggregation [47]. In nonpolar media, both **F-Tri^4** and **O-Tri^1** mono spin-labeled analogs show a fast drop in their $V(T)$ at small T, followed by a slow decay modulated by the dipolar interaction, Fig. 6.3, curves *1* and *2*. Addition of the polar EtOH to the same samples changes the decays to exponential functions, Fig. 6.3, curves *3* and *4*, indicating a disruption of the aggregates into monomers. For both **F-Tri^4** and **O-Tri^1**, $N = 4 \pm 0.3$ spin labels were found in each aggregate and the distances, within an aggregate, between spin labels on different monomers were $r = 2.35$ nm and 2.60 nm.

Similar aggregation phenomena were found in other frozen glassy solutions: $CHCl_3$/toluene, $CHCl_3$/decalin, CCl_4/toluene, and dichloroethane/toluene. The exact quaternary structure that forms depends somewhat on the solvent properties, with r_{max} ranging between 2.3 and 3.3 nm, and N between 3.1 and 4.3 [48]. Doubly spin-labeled trichogin analogs gave consistent results [32]. A model of the aggregate that is consistent with the experimental results contains four peptides arranged as a pair of dimers, Fig. 6.4 [47]. The peptaibols in each dimer are antiparallel. In nonpolar solvents, each peptaibol is a 3_{10}-helix. The tetramer is formed by two dimers. The distances between labels on different peptides are about 2.3 and 2.6 nm, in aggregates of **O-Tri^4** and **O-Tri^1**, respectively. These findings agree well with a helix bundle where the helices are antiparallel. This model of the

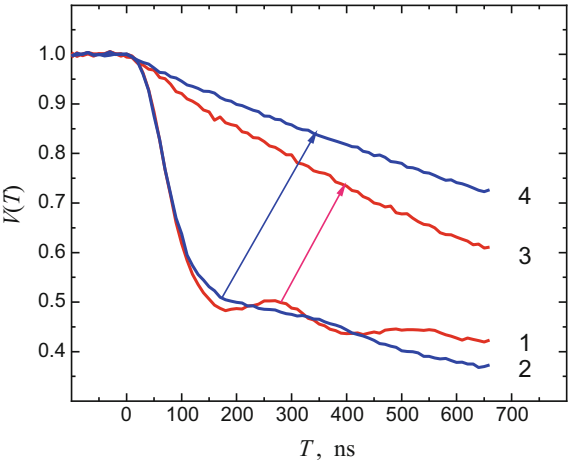

Fig. 6.3 $V(T)$ for mono spin-labeled **F-Tri^4** and **O-Tri^1** in $CHCl_3$/toluene, curves *1* and *2*, respectively, and after addition of EtOH, curves *3* and *4*, respectively; measurements were made at 77 K. Reproduced from Milov et al. [47] with permission of American Chemical Society, copyright 2000

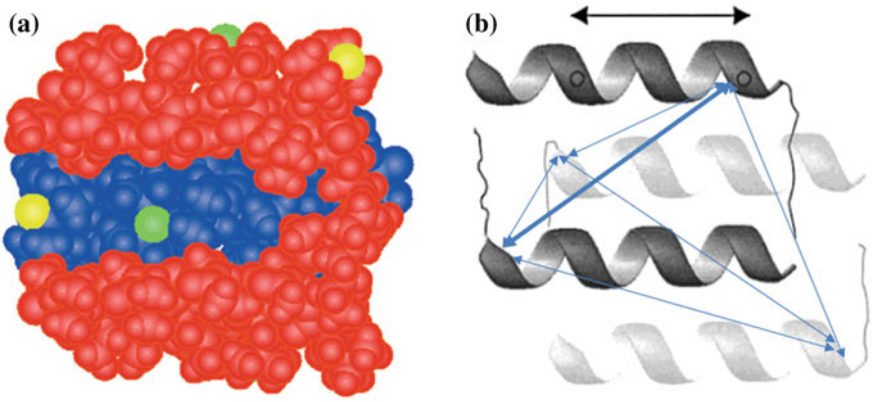

Fig. 6.4 **a** A space-filling molecular model of the quaternary structure of the aggregate of the double spin-labeled **O-Tri**^{1,4} analog in nonpolar media; **b** A ribbon drawing of the supramolecular assembly of one double spin-labeled **O-Tri**^{1,4} and three unlabeled **O-Tri** peptide chains; for clarity, the distances are only shown for the TOAC^{1} positions. Reproduced from Milov et al. [47] with permission of American Chemical Society, copyright 2000

tetramer resembles a vesicle: polar sidechains point to the interior of the tetramer and the nonpolar sidechains to the exterior.

This tetramer model, based on PELDOR experiments, was corroborated by CW EPR data [49, 50]. Two different sets of EPR signals were observed at room temperature in the $CHCl_3$/toluene solvent mixture, which was attributed to an equilibrium between monomers and aggregates. A two-step aggregation mechanism was proposed: dimerization of the peptide molecules, followed by aggregation of the dimers into tetramers. The estimated equilibrium dissociation constant for the first step is ~ 17 μM and for the second step ~ 1 μM. The EPR line widths depend on the rotational mobility of the aggregates and the monomers, which depend on their sizes. Analysis of the line widths gave an estimate of 4 peptide molecules per aggregate,

Tylopeptin B and Heptaibin

The aggregation of tylopeptin B was investigated using tylopeptin B analogs with spin labels at position 3, 8 or 13, Table 6.3. In weakly polar MeOH/toluene solutions, two or three peptide molecules were estimated to make up the aggregates, based on the concentration dependence of the modulation depth [35, 39]. Dimer formation was suggested to be the prevailing mode of self-association with molecules arranged head-to-head. The width of the distance spectrum with the label at the C-terminus in **Tyl**^{13} seems much broader than for **Tyl**^{3} with the label at the N-terminus, suggesting that the C-terminus is more mobile than the N-terminus.

Both head-to-head and head-to-tail dimerization was suggested in heptaibin analogs labeled at position 2 or 14 [35, 39], Table 6.3. The distance distribution spectra contained broad lines, suggesting aggregates containing 3 or 4 peptide molecules, in addition to the dimers.

Table 6.3 Quaternary structures of mono spin-labeled peptaibols in solvent mixtures of low polarity [33]

Peptaibol analog	Label positions	Solvent	N^a	Packing mode	References
O-Tri	1, or 4, or 8	$CHCl_3$/ toluene	4	Antiparallel	[32, 47]
Tyl	3 or 13	MeOH/ toluene	2	Head-to-head[b]	[35, 39]
Hep	2 or 14	MeOH/ toluene	2	Head-to-tail and head-to-head[b]	[35, 39]
Zrv-T^C	C-term	MeOH/ toluene	2	Antiparallel	[21, 22]
Alm	1, or 8, or 16	$CHCl_3$/ toluene	8	Parallel dimer of a linear tetramer	[51, 52]
D-Tri	1, 19	$CHCl_3$/ toluene	2	Antiparallel	[37, 38]

[a]Oligomeric number
[b]Probably a mixture of aggregates of different types

Zervamicin II A

Aggregation of mono spin-labeled zervamicin **Zrv-T^C** molecules was studied in toluene/MeOH mixtures containing 8.5–16% MeOH [21, 22]. The PELDOR $V(T)$ shows a fast decay to a constant limiting value of V_p without any oscillations. This type of trace is characteristic of clusters of electron spins. One can estimate the effective distance r_{eff} between spins in the group from the decay, Sect. 1.2.6. Values of r_{eff} lie between 2.5 and 3.5 nm, depending on solvent. NMR experiments indicate that helical zervamicin molecules in solution have a length of 2.56 nm [6]. Thus, the distance between spin labels at the C-termini of **Zrv-T^C** in the aggregate is consistent with antiparallel arrangements of peptaibols. Moreover, the mean value of $\bar{N}$ calculated from Eq. 1.27 depends on the solvent mixture with $\bar{N} = 2$ for at least 44–67% of **Zrv-T^C** molecules. The sparse 3D-structural information for zervamicin prevents the construction of a detailed molecular model for the aggregate of this peptaibol.

Alamethicin F50/5

Alm analogs spin-labeled at positions 1, 8, or 16 were investigated by CW EPR and PELDOR techniques [51, 52]. The $F(r)$ functions, Fig. 6.5a, from each of the three peptides in $CHCl_3$/toluene (1:1) at concentrations of 10^{-3}–10^{-4} M were remarkably similar. The $F(r)$ functions have a clear, sharp maximum at 3.18 nm for **Alm^1**, 3.24 for **Alm^8**, and 3.06 for **Alm^{16}**, and a much broader maximum near 7 nm. Estimation from the area under regions in *F(r)*, Fig. 6.5a, shows that nearly 30% of the spin labels have the short distances and the remaining 70% have the larger distances. The aggregates seems to contain $N = 6-8$ mol.

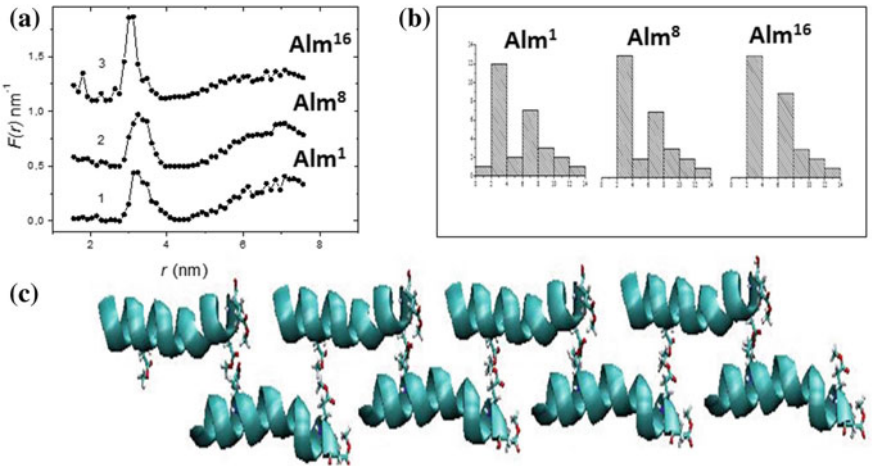

Fig. 6.5 **a** Distance distributions $F(r)$ for mono spin-labeled **Alm**$^{\mathbf{1}}$, **Alm**$^{\mathbf{8}}$, and **Alm**$^{\mathbf{16}}$ aggregates in $CHCl_3$/toluene (1:1) at 77 K, curves *2* and *3* are shifted upwards by 0.5 and 1.1, respectively, to aid comparison; **b** histograms of the distances between labels from MD simulations of an ocatmer model for **Alm**$^{\mathbf{1}}$, **Alm**$^{\mathbf{8}}$, and **Alm**$^{\mathbf{16}}$; the total number of distances determined for each aggregate is 28; **c** a molecular model of an aggregate of **Alm** as an octamer formed as two parallel chains, each composed of four head-to-tail monomers. Reproduced from Milov et al. [51] with permission of John Wiley and Sons, copyright 2007

The CW EPR line shapes of these peptides were studied in chloroform/toluene mixtures at room temperature to obtain a more precise value for N. From the rotational correlation times, N was estimated to be 6.8 ± 2.5 [53]. The combined PELDOR and CW EPR results indicates that $6 \leq N \leq 9$. A model for the **Alm** aggregate was proposed as two linearly aligned tetramers, Fig. 6.5c.

Detailed MD calculations were carried out to test the proposed model. The minimum peptide-peptide interaction energy occurs for molecular conformations in which the Glu γ-ester groups at positions 7, 18, and 19 in both peptides interact as dipoles with antiparallel orientations, thus forming seven polar clusters along the alamethicin aggregate, Fig. 6.5c. This model places the nitroxyl groups on adjacent monomers about 3.3 nm apart. Histograms of the distances between labels, Fig. 6.5b, for this model are in qualitative agreement with the experimental $F(r)$ for the mono spin-labeled **Alm**$^{\mathbf{1}}$, **Alm**$^{\mathbf{8}}$, and **Alm**$^{\mathbf{16}}$.

Dimer of Trichogin GA IV

In this peptide, the sequence of trichogin repeats twice to form a head to tail, covalently-linked dimer, rather than an antiparallel dimer seen in many of the peptaibol aggregates that form in solution. This makes it the longest peptaibol ($n = 22$) studied by PELDOR [37, 38]. The aggregate of the mono spin-labeled **D-Tri**$^{\mathbf{1}}$ has $N \sim 2$, based on V_p, and a distance of 3.4 nm between the spin labels of different molecules. This result implies an antiparallel arrangement of molecules in the aggregate. The estimated total dipole moment of the **D-Tri**$^{\mathbf{1}}$ α-helix is 77.0

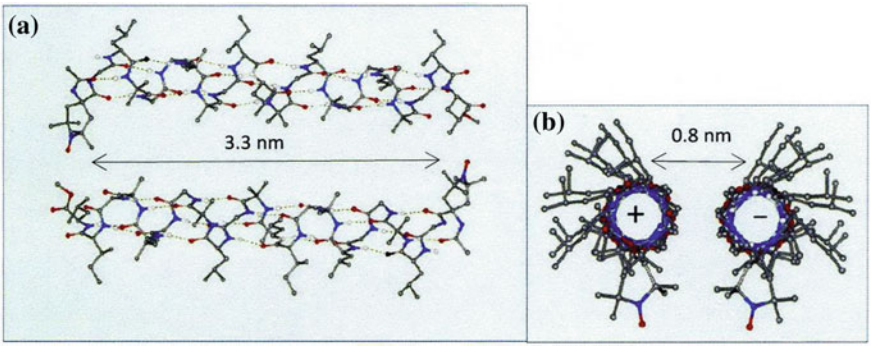

Fig. 6.6 **a** 3D-Structural model of the **D-Tri**[1] aggregate: molecules with an antiparallel orientation and a label-label distance in the dimer of 3.3 nm and **b** a view along the axes of the α-helices; the centers of the two helices are separated by about 0.8 nm. Reproduced from Milov et al. [37] with permission of American Chemical Society, copyright 2003

Debye, aligned along the helix. This large electric dipole strongly favors the antiparallel arrangement, while the distance between α-helices is determined only by steric factors. A 3D-structural model for the **D-Tri**[1] peptide aggregate was based on these results, Fig. 6.6.

6.1.3 *Secondary Structures in Membrane Systems*

Trichogin GA IV

Trichogin GA IV has a remarkable ability to modify cell membranes even though its length is much less than the thickness of a membrane [1, 2, 4]. Detailed information about its aggregation state in the membrane is needed to understand how this short peptide produces such a dramatic effect on membrane permeability. The experimental distance distribution function of **F-Tri**[1] aggregates in a model membrane composed of DPPC (1,2-dipalmitoyl-*sn*-glycero-3-phosphocholine) lipid bilayers exhibits a maximum near 2.5 nm and a half width of 1.4 nm, Fig. 6.7. This is a broad distance distribution, suggesting that several different types of aggregates form. At 5 mol% peptide relative to the DPPC in the bilayers, aggregates are mostly pairs of trichogin molecules with $N = 2.1 \pm 0.1$. In other solvents, N for the spin-labeled trichogin was 1, i.e., a monomer, in the polar solvent EtOH or 4.3, a tetramer, in nonpolar dichloroethane/toluene.

Experiments with fluorescent trichogin analogs at much lower concentrations in large unilamellar vesicles, or LUVs, composed of egg phosphatidyl choline (ePC) and cholesterol gave a lower limit of $N = 2.3$ mol per aggregate [54], while the rate-limiting step for ion conduction in ePC LUVs with cholesterol involves 3–4 unlabeled trichogin molecules at a similar concentration [55]. For peptide

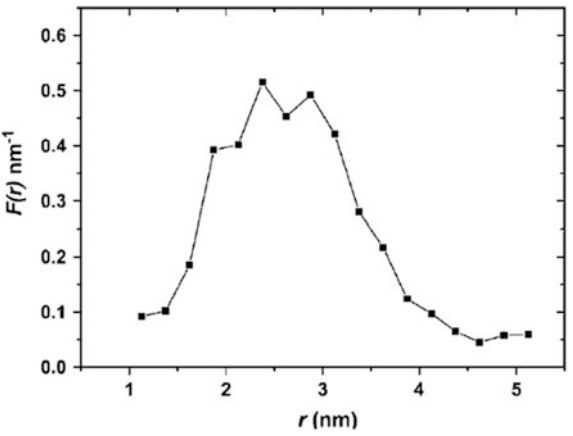

Fig. 6.7 Distance distribution spectra $F(r)$ for spin labels of **F-Tri**[1] aggregates in DPPC lipid bilayers. Reproduced from Milov et al. [56] with permission of Springer, copyright 2005

concentrations of 0.5–2.2 mol% in ePC vesicles, PELDOR studies showed that **O-Tri**[4] is distributed homogeneously in the membranes [56, 57], but the distribution became inhomogeneous and aggregates formed upon addition of cholesterol. The cholesterol seems to stabilize aggregates in the model membranes.

Crystallographic data for trichogin GA IV shows a mixed 3_{10}-/α-helix structure for the peptide backbone [7, 8]. Since the α- and 3_{10}-helices have different lengths, PELDOR can determine the conformation in the membrane from the distance between labels on the same molecule [37, 38, 56–58]. The distance distribution function $F(r)$ was measured for the double spin-labeled **F-Tri**[1,8] in ePC membranes, Fig. 6.8a, [56]. Two main maxima occur at distances of 1.25 and 1.77 nm, corresponding to the α- and 3_{10}-helical conformations, respectively. Apparently, each trichogin molecule is in one of two conformations, with the α-helix being more common. The distance distribution function for **O-Tri**[1,8] in DPPC membranes [58] also corresponds to a mixture of α- and 3_{10}-helix populations, but with the 3_{10}-helix favored, Fig. 6.8b.

In both ePC and DPPC membranes, the trichogins were monomers in the PC head-group regions of the membranes [58]. Thus, the different ratios of helix populations in the two membranes cannot be caused by a different molecular environment, e.g., polar head group versus hydrophobic core, or by a different aggregation state. The trichogin analogs used with the two membrane models are capped at the N-terminus by different groups, i.e., the Fmoc group in **F-Tri**[1,8] and the Oct group in **O-Tri**[1,8]. The Fmoc is a fused, rigid aromatic moiety, while the Oct group has a long, very flexible hydrocarbon chain. Capping a peptide on the N-terminus is well-known to stabilize the helical conformation [27], but the physical basis for the dramatically different helix populations in Fig. 6.8 remains unclear and deserves further investigation.

The spatial distribution of the mono-labeled trichogin GA IV **O-Tri**[4] in spherical cell membranes of the Gram-positive bacterium *Micrococcus luteus* are discussed in Sect. 5.4.

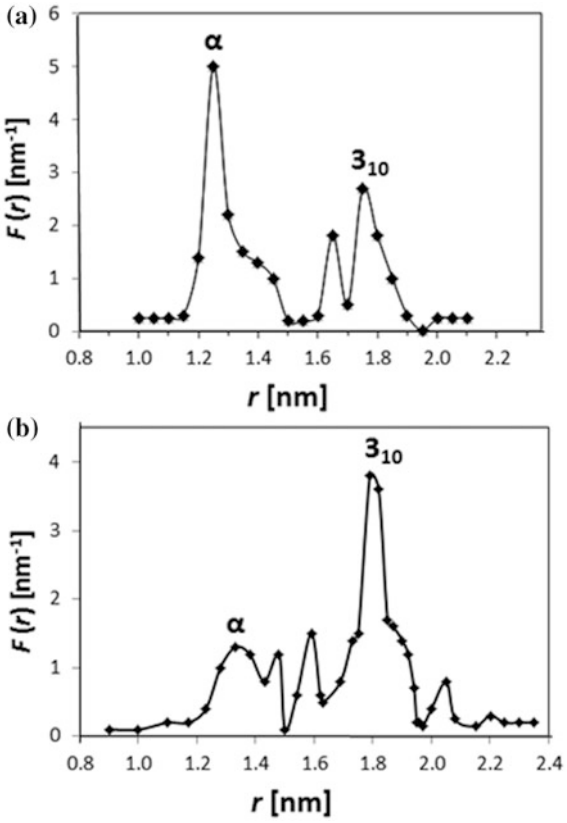

Fig. 6.8 $F(r)$ obtained for **a** **F-Tri**^{1,8} in ePC; and **b** **O-Tri**^{1,8} in DPPC membranes. Reproduced from Milov et al. [58] with permissions of Royal Society of Chemistry, copyright 2004

Alamethicin F50/5

Self-assembled aggregates of **Alm** were studied in vesicle membranes at peptide to lipid molar ratios in the range 1:70–1:200. The intermolecular distance distribution was obtained from mono spin-labeled peptides at 77 K, and the aggregation number was estimated as $N \approx 4$ [59–62]. The distance distributions have similar maxima near 2.3 nm. **Alm**^{16} had no other peaks, while **Alm**^{1} and **Alm**^{8} had additional maxima at 3.2 and $\sim$5.2 nm, Fig. 6.9.

Two important features are that these distributions are independent of the spin label position, and they have maxima of $\sim$2.3 nm. These agree well with a simple model of parallel, face-to-face helices with polar groups oriented to the inside and the spin labels to the outside of the aggregate. But these results are inconsistent with an antiparallel orientation of helices which would place the TOAC labels of **Alm**^{16} 3.4 nm apart, well beyond the experimental $F(r)$ peak, Fig. 6.9 curve *3*.

A molecular modeling study was carried out to gain greater insight into the helix-helix interactions [62]. The modeling used the intermolecular PELDOR $F(r)$ between TOAC labels as distance restraints. Each peptide molecule was modeled

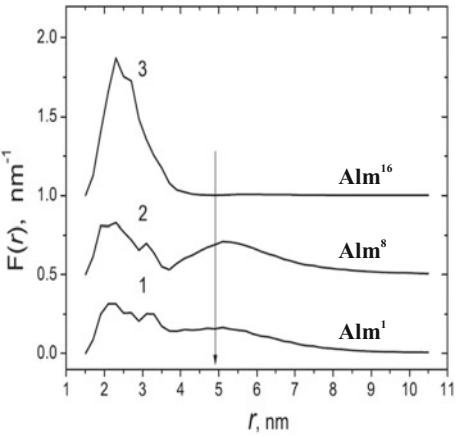

Fig. 6.9 Distance distribution $F(r)$ between TOAC spin-labels for **Alm** analogs in membranes of frozen ePC vesicles; for clarity, curves *2* and *3* are shifted upward by 0.5 and 1.0, respectively, the shape of $F(r)$ at distances longer than that indicated by the arrow is not real and can be used only for estimation of the area under the broad line. Reproduced from Milov et al. [62] with permissions of Elsevier, copyright 2009

with TOAC labels at positions 1, 8, and 16, so that only a single structure had to be optimized but distances could be calculated for all three mono-labeled analogs. The gas-phase, energy-minimized peptide complex has four parallel, but slightly tilted, α-helices, Fig. 6.10. The α-helical structure is broken near the center of each peptide by Pro^{14}. A similar break was also found in a ^{1}H-NMR study of micelle-associated **Alm** [63].

The intramolecular distances between the TOAC residues of **Alm^{1,16}** were not constrained in the model, and confirmed the α-helical conformation in the aggregate [62]. An earlier PELDOR study of doubly spin-labeled **Alm^{1,16}** aggregates in ePC membranes found an average distance of 2.1 nm with a deviation of 0.5 nm between intramolecular labels at peptide to lipid ratios of 1:50 or 1:200 [36]. This experimental distance agrees with the model within experimental error. Thus, the membrane-bound peptides are α-helical despite the disruption by Pro^{14}. Close examination shows that the intermolecular distance of 1.8 nm between the nitroxyl oxygen atoms of the **Alm^{1}** residues matches the first peak of the PELDOR experiments, but not the maximum at 2.3 nm. It should not be a surprise that a gas-phase structural model fails to reproduce every detail of a membrane-embedded protein complex.

This model structure can be accommodated in the hydrophobic region of the membrane by orienting the N-terminal helices of the blue and red colored chains with tilt angles of 15°, the cyan chain by 13°, and the yellow by 8° from the membrane normal, Fig. 6.10. Similar tilts were found for **Alm** by EPR and solid-state NMR analyses [64, 65]. The blue, red, and yellow transmembrane helices extend ∼3.2 nm, This is a good match to the ∼3.5 nm hydrophobic

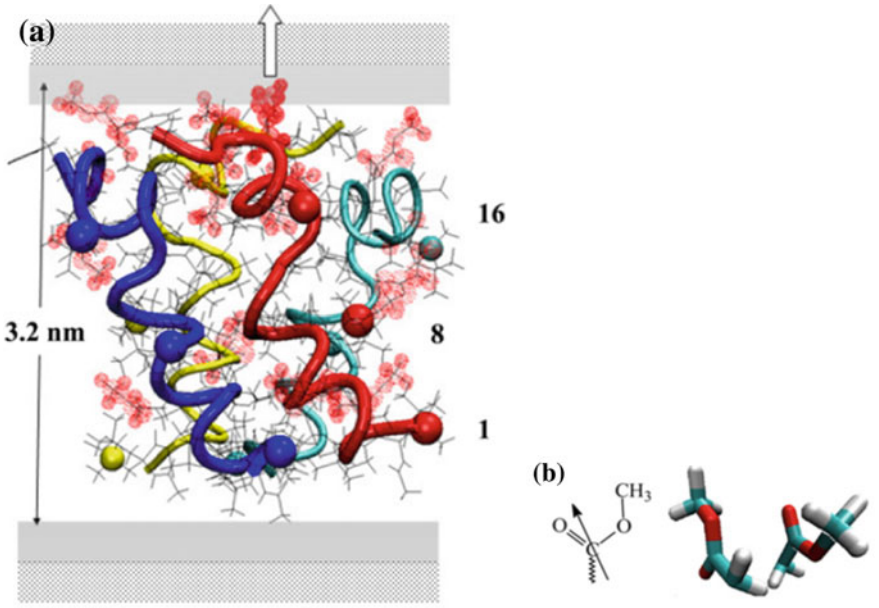

Fig. 6.10 **a** Energy-minimized model of a triply-labeled **Alm** tetramer, based on the short 2.3 nm PELDOR distance between nitroxyl oxygen atoms (indicated by balls) of singly-labeled **Alm**$^{\mathbf{1}}$, **Alm**$^{\mathbf{8}}$, and **Alm**$^{\mathbf{16}}$; numbers on the right-hand side indicate the approximate membrane depth of the corresponding labeled position; each helix is interrupted at Pro^{14}; **b** relative positions of ester groups at the end of Glu^{18}sidechains; for clarity, only one pair is shown; strong electric dipole-dipole interactions between ester groups stabilize the helix bundle and seem to anchor the aggregate to the polar region of the membrane. Reproduced from Milov et al. [62] with permissions of Elsevier, copyright 2009

thickness of the ePC membrane, Fig. 6.10a, in view of the uncertainty in the thickness of the membrane [66, 67] and the possibility of peptide-induced membrane thinning effects [68]. The C-terminus of the cyan chain in this model is immersed more deeply in the hydrophobic region of the membrane.

The polar Glu(OMe) [7, 8, 69] residues of **Alm** seem to have an important role in the closed, or non-conducting, state of the **Alm** channel. Their approximate positions are indicated by dotted circles in Fig. 6.10a, taking into account the flexibility of the long γ-ester side chains. The Glu^{18}(OMe) γ-esters of the red and cyan molecules are only 0.36 nm apart, Fig. 6.10b. Electric dipole-dipole interactions between these γ-ester groups were key in stabilizing aggregates of **Alm** in hydrophobic solvents. It seems that interactions of the C-termini play a similar role in aggregate formation in the ePC membrane. In addition, four of the eight Glu (OMe) groups at the C-terminal are in or near the polar region of the membrane, Fig. 6.10a. This suggests a role for the γ-ester groups of the Glu(OMe) [8] residues in anchoring the aggregate to the polar region of the membrane via dipole-dipole interactions with ester groups of the lipid.

6.1.4 Peptaibols on Surfaces

Peptides absorbed on inorganic or organic surfaces are important in many interdisciplinary areas, such as nanotechnology, biotechnology, medicine, food production, tissue engineering and geochemistry. The properties of absorbed peptides are determined by the primary and secondary structures of the peptides, the nature of the surface, and the type of interaction at the peptide-surface interface.

NMR studies of such systems has achieved some remarkable successes [70, 71]. Solid-state NMR studies of dipolar interactions between magnetic nuclei in a peptide can establish the conformation and orientation of the peptide on different sorbents. Similarly, EPR and PELDOR studies of dipole-dipole interactions in spin-labeled peptides provides information on peptide conformations and aggregation motifs on various types of surfaces. One such PELDOR study of alamethicin absorbed on organic and inorganic sorbents illustrates this.

On HLB

We saw earlier in this chapter that the secondary structure of alamethicin F50/5, or **Alm**, is rather sensitive to the molecular properties of its environment and this holds true for **Alm** on surfaces. Mono and doubly spin-labeled analogs were used as absorbates: **Alm^{1}**, **Alm^{16}**, **Alm^{1,16}**, Table 6.1 [72]. The polymeric, reverse-phase organic sorbent Oasis HLB was the surface. HLB has both hydrophilic and lipophilic properties, and is widely used as the solid phase for liquid chromatography. The peptides were absorbed onto HLB from methylene chloride solution and dried under a flow of dry nitrogen. The amount absorbed was measured at 77 K by CW-EPR.

Intra- and intermolecular contributions to the PELDOR $V(T)$ were separated, taking into account the actual fractal dimensionality of the system. The $V_{\mathrm{INTER}}(T)$ showed a fractal dimensionality d of 2.6 and not the 2.0 expected for an ideal planar surface, Sect. 1.2.4. This indicates that the surface of HLB itself has some fractal character. The $V(T)$ indicate aggregation of **Alm** on HLB. The background–corrected $V(T)$ were analyzed using Tikhonov regularization, Fig. 6.11. Solutions of **Alm^{1,16}** in ethanol were used as a convenient reference.

The distance distributions for **Alm^{1,16}** in ethanol and on HLB, Fig. 6.11, curves *1* and *2*, respectively, are asymmetric. In ethanol, $r_{max} = 2.00 \pm 0.02$ nm and the width at half-height is $\Delta = 0.25 \pm 0.03$ nm. The distance distribution for the absorbed **Alm^{1,16}** is much broader, $\Delta = 0.75 \pm 0.1$ nm, although the peak position is virtually identical, $r_{max} = 2.00 \pm 0.03$ nm [72]. The 2.0 nm distance corresponds to an α-helical conformation. The tail of the peak in ethanol extending to longer distances is probably due to a minor fraction of peptides having elongated $\alpha/3_{10}$-helix conformations with distances in the range $2.0 < r < 2.7$ nm, Fig. 6.11. The fraction of these conformers increases substantially when the peptide is absorbed on HLB. The broadening of the main line with $r_{max} = 2.00$ nm and an increase in the elongated conformers are likely due to the greater diversity in peptide surroundings on HLB as compared to the frozen ethanol.

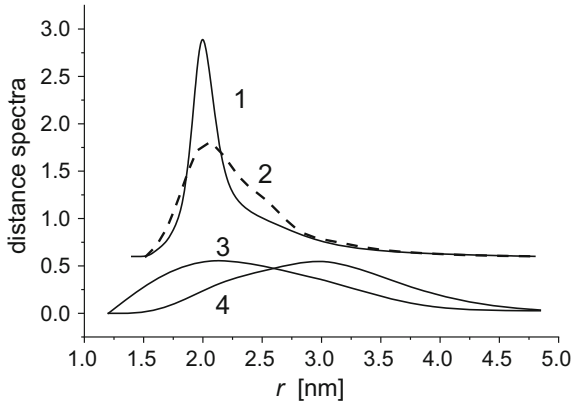

Fig. 6.11 Intramolecular $F(r)$ between TOAC spin labels in **Alm**^{1,16} and intermolecular $F(r)$ between TOAC labels in **Alm** aggregates: Curves *1* and *2* are from **Alm**^{1,16} in ethanol and on HLB, respectively, Curves *3* and *4* are from aggregates of mono-labeled **Alm**^{16} and **Alm**^{1} on HLB, respectively, Curves *1* and *2* are shifted upward by 0.6. Reproduced from Milov et al. [72] with permissions of American Chemical Society, copyright 2014

The $F(r)$ maximum between labels in aggregates on HLB depends on the position of the label. The $r_{max} = 2.1 \pm 0.1$ nm for **Alm**^{16} on HLB shifts to $r_{max} = 3.0 \pm 0.1$ nm for **Alm**^{1}, Fig. 6.11 curves *3* and *4*, respectively. This shift suggests that **Alm** forms aggregates with the C-terminal regions near each other. However, the distance distribution between labels at either position is remarkably broad, $\Delta = 1.6 \pm 0.1$ nm.

On silica nanospheres

Doubly spin-labeled peptaibols have been studied absorbed onto monodisperse silica (SiO_2) nanospheres about 20 nm in diameter. One was the short trichogin, **Tri**^{1,8}, and the other a medium-length ampullosporin, **Amp**^{3,13}, Table 6.1 [73].

The EPR spectra of **Tri**^{1,8} broadened upon absorption, showing that trichogin forms closely-packed peptide clusters. Washing the surface with excess solvent, dispersed the clusters into non-aggregated, surface-bound peptides that can be studied by PELDOR. The PELDOR time traces of the absorbed peptides indicate a fractal dimensionality $d = 2.1$, corresponding to absorption on a fairly planar surface. The distance distribution maximum around $r_{max} \sim 1.9$ nm for absorbed **Tri**^{1,8} was about the same as in methanol solution, with width $\Delta = 0.6$ nm, implying little change in their helical configuration.

In contrast, **Amp**^{3,13} has significantly different conformations in frozen solution and when absorbed. The $F(r)$ peak increases from 1.73 nm in methanol to 2.25 nm when absorbed on silica nanospheres and the width of the distance distribution increases greatly from 0.05 to 0.8 nm, Fig. 6.12. We can conclude that **Tri**^{1,8} remained a $2.2_7/3_{10}$ helix after absorption, but the **Amp**^{1,13} $F(r)$ is so broad that it is compatible with all helix conformations and even a β sheet, Fig. 6.1.

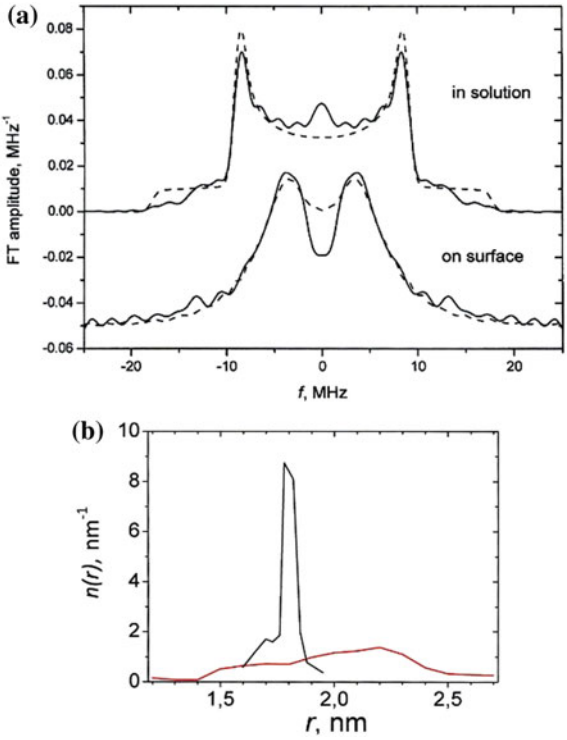

Fig. 6.12 **a** Cosine Fourier transforms (solid lines) and their simulations (*dashed lines*); and **b** $F(r)$ of the experimental $V_N(T)V_N(T)$ for **Amp**[3,13] in frozen methanol and absorbed on silica nanospheres; the spectra for the absorbed sample in **a** are shifted downward by 0.05 MHz^{-1} for convenience. Reproduced from Syryamina et al. [73] with permission of Springer, copyright 2016

6.2 Spin-Labeled Alanine- and Proline-Based Peptides

The accuracy and precision, with which PELDOR techniques measure distances and peptide conformations, was verified with a series of well-characterized doubly spin-labeled peptides [74]. The peptides were based on a repeating sequence of four alanine and one lysine amino acid residues: $(A{\cdot}A{\cdot}A{\cdot}A{\cdot}K)_n{\cdot}A$ with $n = 4$ or 7. The sequence is written here with the standard, single-letter notation with lysine, alanine and cysteine amino acid residues indicated by K, A and C, respectively. Specific alanine residues were replaced by cysteine residues to which MTS **4-12** or SAT **4-15** spin labels were attached. The labeled peptides are indicated by the value of n and the positions of the labeled cysteines. For example, 4K(3, 7) indicates the sequence of **6-1**, Table 6.4.

A wide range of peptides from 4K(3, 7) up to 7K(3, 32) were studied. The CW-EPR lineshape at X-band and the 4pPELDOR signals were measured at 50 K in frozen aqueous solutions. The limited pulse bandwidth produced some distortion at the shorter inter-spin distances, so the variation of the PELDOR modulation depth with pump pulse length was used to help correct the measured distances [74]. The resulting distances were compared with MD calculations that assume an

Table 6.4 Amino acid sequences of alanine- and proline-rich peptides investigated by PELDOR spectroscopy; the label sites are indicated by bold characters[a]

	Sequence
6-1	A·A·**C**·A·K·A·**C**·A·A·K·A·A·A·A·K·A·A·A·A·K·A[b]
6-2	Ac-A·A·A·A·K·(**TOPP**)·A·K·A·A·A·A·A·K·A·A·K·A·(**TOPP**)·K·A·A·A·A-NH_2
6-3	Ac-A·A·A·A·K·($\mathbf{C_{MTSSL}}$)·A·K·A·A·A·A·A·K·A·A·K·A·($\mathbf{C_{MTSSL}}$)·K·A·A·A·A-NH_2
6-4	P·**P**·**H**·**G**·**G**·**G**·**W**·P·P·P·P·P·P·P·**P**·**H**·**G**·**G**·**G**·**W**
6-5	P·**P**·**H**·**G**·**G**·**G**·**W**·P·A·A·A·A·K·A·A·A·A·K·($\mathbf{C_{MTSSL}}$)·A·A·A·A·K·A

[a]Standard, single-letter amino acid codes are used: *P* proline; *H* histidine; *G* glycine; *W* tryptophan; *A* alanine; *K* lysine; *C* cysteine
[b]This sequence is corresponds to 4K(3, 7) in the text

α-helical structure of the peptide. Eight peptides with $n = 4$ and one peptide with $n = 7$ provided EPR and PELDOR data at distances between 1.0 and 4.7 nm.

There is a strong correlation between the experimental and modeled mean distances, Fig. 6.13, which even extends to 4.7 nm for 7K(3, 32). PELDOR provided excellent agreement for distances greater than 2.0 nm. Corrections for pulse bandwidth limitations extended that lower bound to near 1.6 nm. A large part of the 'error bars' in Fig. 6.13 is due to the range of conformations that was present in liquid solution and that was preserved when the sample was frozen. Unfortunately, the figure does not indicate the distribution of distances from the MD modeling of the liquid solutions.

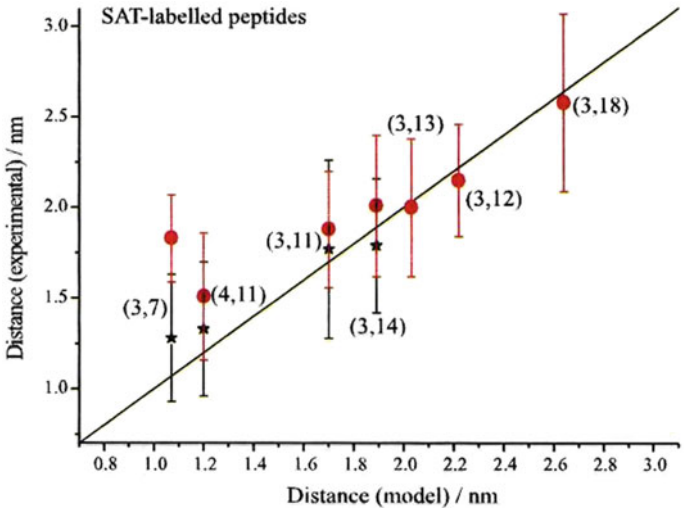

Fig. 6.13 Average distance and standard deviation from dipolar lineshape analysis (star) and PELDOR (red circle) for the SAT label on 4K(i, j) peptides; the model distance is the mean distance between spin labels from MD simulations. Reproduced from Banham et al. [74] with permissions of Elsevier, copyright 2008

The upper bound for CW-EPR measurements is in the range 1.5–1.7 nm. Exchange coupling and inhomogeneous EPR line broadening are a major source of errors in the overlap region near 1.5 nm where both CW-EPR and PELDOR are reliable. CW EPR spectroscopy and PELDOR techniques reliably measured distances in the alanine peptides spanning a wide range from 1.07 to over 4.6 nm [74].

The 4K family of alanine-based peptides are α-helical in aqueous solutions according to MD modeling and NMR and CD data but the helix is not rigid. The 7K peptide also seemed to be α-helical but PELDOR gave a somewhat shorter mean distance and broader distribution than expected for a completely rigid helix [74].

Two alanine-rich peptides, **6-2** and **6-3**, Table 6.4, labeled by TOPP **4-21** and Cys-MTSL **4-16** were synthesized and studied by X-band PELDOR in frozen solutions of TFE/EtOH/H_2O and TFE/EtOH/MeOH at 50 K. Tikhonov analysis of the PELDOR $V(T)$ of **6-2** indicated a narrow distance distribution centered at 2.80 nm having a width $\Delta = 0.26$ nm. The distance is consistent with the estimate of 2.7 nm for two rigid spin labels linked to an α-helical peptide. A comparative study of peptide **6-3** gave an interspin distance of 2.26 nm, with a width as narrow as that of **6-2** [75]. MTSL labels usually give broad distance distributions, yet the observed distance between the MTSL is over 0.5 nm shorter than the distance between TOPP labels. These anomalies suggest that the MTSL labels may adopt a specific conformation in this peptide. This highlights a major advantage with the use of TOPP rather than MTSL: the interpretation of the distance is straightforward due to the rigid, reliable structure of the label. Unfortunately, the potential for orientation selection with the rigid TOPP labels was not exploited to determine their mutual orientation in the peptide.

Peptide chains have been used as linkers between paramagnetic ions and nitroxyls. Measurements of Cu^{2+}–Cu^{2+} and Cu^{2+}–nitroxyl distance distributions used PELDOR with a proline-based peptide **6-4** and an alanine-based peptide **6-5**, Table 6.4 [76, 77]. The proline-based peptide contains two well-characterized Cu^{2+} binding segments, P·H·G·G·G·W, separated by seven proline residues. Again, standard, single-letter amino acid codes are used: P, proline; H, histidine; G, glycine; W, tryptophan; A, alanine; K, lysine; C, cysteine. The P·H·G·G·G·W sequence in both peptides is a copper-binding sequence, while cysteine near one end of **6-5** was used to covalently attach the MTSL spin label. The P·H·G·G·G·W sites were occupied by Cu^{2+}.

PELDOR experiments were performed at several applied magnetic fields and resonance offsets to probe orientation selection effects on the Cu^{2+}-based PELDOR signal. Subtle orientation selection was observed from the PELDOR spectra of both peptides [76, 77]. A general theoretical model based on [78] was used to analyze the experimental data. Tikhonov regularization did not extract precise Cu^{2+}-based distance distributions. Instead, a full data analysis was required to obtain the distance distributions and relative orientations with a 3.0 nm mean Cu^{2+}−Cu^{2+} distance and a 2.7 nm mean Cu^{2+}-nitroxyl distance in the two peptides. These distances are consistent with structural models and with earlier measurements [79].

Constraints on the relative orientation between paramagnetic centers in these two model peptides were determined by examination of orientation selection effects. The analysis procedure is system independent, and therefore is applicable to more complicated biological systems.

References

1. Toniolo C, Crisma M, Formaggio F, Peggion C, Epand RF, Epand RM (2001) Lipopeptaibols, a novel family of membrane active, antimicrobial peptides. Cell Mol Life Sci 58(9):1179–1188. https://doi.org/10.1007/Pl00000932
2. Peggion C, Formaggio F, Crisma M, Epand RF, Epand RM, Toniolo C (2003) Trichogin: a paradigm for lipopeptaibols. J Pept Sci 9(11–12):679–689. https://doi.org/10.1002/psc.500
3. Toniolo C, Crisma M, Formaggio F, Peggion C, Monaco V, Goulard C, Rebuffat S, Bodo B (1996) Effect of *N*-alpha-acyl chain length on the membrane-modifying properties of synthetic analogs of the lipopeptaibol trichogin GA IV. J Am Chem Soc 118(21):4952–4958. https://doi.org/10.1021/ja954081o
4. Rebuffat S, Goulard C, Bodo B, Roquebert MF (1999) The peptaibol antibiotics from *Trichoderma* soil fungi; structural diversity and membrane properties. In: Pandalai SG (ed) Recent research developments in organic & bioorganic chemistry, vol 3. Transworld Research Network, Trivandrum, pp 65–91
5. Fox RO, Richards FM (1982) A voltage-gated ion channel model inferred from the crystal-structure of alamethicin at 1.5 Å resolution. Nature 300(5890):325–330. https://doi.org/10.1038/300325a0
6. Karle IL, Flippenanderson J, Sukumar M, Balaram P (1987) Conformation of a 16-residue zervamicin-iia analog peptide containing 3 different structural features—3(10)-helix, alpha-helix, and beta-bend ribbon. Proc Natl Acad Sci USA 84(15):5087–5091. https://doi.org/10.1073/pnas.84.15.5087
7. Toniolo C, Peggion C, Crisma M, Formaggio F, Shui XQ, Eggleston DS (1994) Structure determination of racemic trichogin-a-IV using centrosymmetric crystals. Nat Struct Biol 1 (12):908–914. https://doi.org/10.1038/nsb1294-908
8. Crisma M, Monaco V, Formaggio F, Toniolo C, George C, Flippen-Anderson JL (1997) Crystallographic structure of a helical lipopeptaibol antibiotic analogue. Lett Pept Sci 4(4–6):213–218. https://doi.org/10.1023/A:1008874816982
9. Toniolo C, Brückner H (2007) Topical issue: peptaibiotics. Chem Biodivers 4(6):1021–1412. https://doi.org/10.1002/cbdv.200790093
10. Brückner H, Toniolo C (2013) Special issue: peptaibiotics II. Chem Biodivers 10(5):731–961. https://doi.org/10.1002/cbdv.201300139
11. Toniolo C, Brückner H (eds) (2009) Peptaibiotics fungal peptides containing α-dialkyl α-amino acids. Wiley-VCH, Weinheim
12. Toniolo C, Crisma M, Formaggio F, Peggion C (2001) Control of peptide conformation by the thorpe-ingold effect (C(alpha)-tetrasubstitution). Biopolymers 60(6):396–419. https://doi.org/10.1002/bip.10184
13. Karle IL, Balaram P (1990) Structural characteristics of alpha-helical peptide molecules containing aib residues. Biochem US 29(29):6747–6756. https://doi.org/10.1021/bi00481a001
14. Toniolo C, Crisma M, Formaggio F (1998) TOAC, a nitroxide spin-labeled, achiral C(alpha)-tetrasubstituted alpha-amino acid, is an excellent tool in material science and biochemistry. Biopolymers 47(2):153–158

15. Hanson P, Millhauser G, Formaggio F, Crisma M, Toniolo C (1996) ESR characterization of hexameric, helical peptides using double TOAC spin labeling. J Am Chem Soc 118 (32):7618–7625. https://doi.org/10.1021/ja961025u
16. Hanson P, Anderson DJ, Martinez G, Millhauser G, Formaggio F, Crisma M, Toniolo C, Vita C (1998) Electron spin resonance and structural analysis of water soluble, alanine-rich peptides incorporating TOAC. Mol Phys 95(5):957–966. https://doi.org/10.1080/002689798166576
17. Anderson DJ, Hanson P, McNulty J, Millhauser G, Monaco V, Formaggio F, Crisma M, Toniolo C (1999) Solution structures of TOAC-labeled trichogin GA IV peptides from allowed ($g \approx 2$) and half-field electron spin resonance. J Am Chem Soc 121(29):6919–6927. https://doi.org/10.1021/ja984255c
18. Bobone S, Roversi D, Giordano L, De Zotti M, Formaggio F, Toniolo C, Park Y, Stella L (2012) The lipid dependence of antimicrobial peptide activity is an unreliable experimental test for different pore models. Biochem US 51(51):10124–10126. https://doi.org/10.1021/bi3015086
19. Bobone S, Gerelli Y, De Zotti M, Bocchinfuso G, Farrotti A, Orioni B, Sebastiani F, Latter E, Penfold J, Senesi R, Formaggio F, Palleschi A, Toniolo C, Fragneto G, Stella L (2013) Membrane thickness and the mechanism of action of the short peptaibol trichogin GA IV. BBA-Biomem 1828(3):1013–1024. https://doi.org/10.1016/j.bbamem.2012.11.033
20. Tsvetkov YD, Milov AD, Maryasov AG (2008) Pulsed electron–electron double resonance (PELDOR) as EPR spectroscopy in nanometre range. Russ Chem Rev 77(6):487–520
21. Milov AD, Tsvetkov YD, Gorbunova EY, Mustaeva LG, Ovchinnikova TV, Raap J (2002) Self-aggregation properties of spin-labeled zervamicin IIA as studied by PELDOR spectroscopy. Biopolymers 64(6):328–336. https://doi.org/10.1002/bip.10208
22. Milov AD, Tsvetkov YD, Gorbunova EY, Mustaeva LG, Ovchinnikova TV, Handgraaf JW, Raap J (2007) Solvent effects on the secondary structure of the membrane-active zervamicin determined by PELDOR spectroscopy. Chem Biodivers 4(6):1243–1255. https://doi.org/10.1002/cbdv.200790107
23. Toniolo C, Benedetti E (1991) The polypeptide-3_{10}-helix. Trends Biochem Sci 16(9):350–353
24. Yasui SC, Keiderling TA, Bonora GM, Toniolo C (1986) Vibrational circular-dichroism of polypeptides. 5. A study of 3_{10}-helical-octapeptides. Biopolymers 25(1):79–89. https://doi.org/10.1002/bip.360250107
25. Crisma M, Formaggio F, Moretto A, Toniolo C (2006) Peptide helices based on alpha-amino acids. Biopolymers 84(1):3–12. https://doi.org/10.1002/bip.20357
26. Toniolo C (1980) Intramolecularly hydrogen-bonded peptide conformations. CRC Cr Rev Bioch Mol 9(1):1–44. https://doi.org/10.3109/10409238009105471
27. Crisma M, De Zotti M, Moretto A, Peggion C, Drouillat B, Wright K, Couty F, Toniolo C, Formaggio F (2015) Single and multiple peptide gamma-turns: literature survey and recent progress. New J Chem 39(5):3208–3216. https://doi.org/10.1039/c4nj01564a
28. Armen R, Alonso DOV, Daggett V (2003) The role of α-, 3_{10}-, and π-helix in helix → coil transitions. Protein Sci 12(6):1145–1157. https://doi.org/10.1110/ps02040103
29. Millhauser GL (1995) Views of helical peptides—a proposal for the position of 3_{10}-helix along the thermodynamic folding pathway. Biochem US 34(12):3873–3877. https://doi.org/10.1021/bi00012a001
30. Milov AD, Maryasov AG, Tsvetkov YD, Raap J (1999) Pulsed ELDOR in spin-labeled polypeptides. Chem Phys Lett 303(1–2):135–143. https://doi.org/10.1016/S0009-2614(99)00220-1
31. Milov AD, Maryasov AG, Samoilova RI, Tsvetkov YD, Raap J, Monaco V, Formaggio F, Crisma M, Toniolo C (2000) Pulsed double electron–electron resonance in spin-labeled polypeptides data on the secondary structure. Dokl Akad Nauk 370(2):265–268

32. Milov AD, Tsvetkov YD, Formaggio F, Crisma M, Toniolo C, Raap J (2001) The secondary structure of a membrane-modifying peptide in a supramolecular assembly studied by PELDOR and CW-ESR spectroscopies. J Am Chem Soc 123(16):3784–3789. https://doi.org/10.1021/ja0033990
33. Milov AD, Tsvetkov YD, Raap J, De Zotti M, Formaggio F, Toniolo C (2016) Conformation, self-aggregation, and membrane interaction of peptaibols as studied by pulsed electron double resonance spectroscopy. Biopolymers 106(1):6–24. https://doi.org/10.1002/bip.22713
34. Milov AD, Tsvetkov YD, Maryasov AG, Gobbo M, Prinzivalli C, De Zotti M, Formaggio F, Toniolo C (2012) Conformational properties of the spin-labeled tylopeptin B and heptaibin peptaibiotics based on PELDOR spectroscopy data. Appl Magn Reson 44(4):495–508. https://doi.org/10.1007/s00723-012-0402-1
35. Milov AD, Tsvetkov YD, De Zotti M, Prinzivalli C, Biondi B, Formaggio F, Toniolo C, Gobbo M (2013) Aggregation modes of the spin mono-labeled tylopeptin B and heptaibin peptaibiotics in frozen solutions of weak polarity as studied by PELDOR spectroscopy. J Struct Chem 54:S73–S85. https://doi.org/10.1134/S0022476613070056
36. Milov AD, Samoilova RI, Tsvetkov YD, De Zotti M, Toniolo C, Raap J (2008) PELDOR conformational analysis of bis-labeled alamethicin aggregated in phospholipid vesicles. J Phys Chem B 112(43):13469–13472. https://doi.org/10.1021/Jp8046714
37. Milov AD, Tsvetkov YD, Formaggio F, Oancea S, Toniolo C, Raap J (2003) Aggregation of spin labeled trichogin GA IV dimers: distance distribution between spin labels in frozen solutions by PELDOR data. J Phys Chem B 107(49):13719–13727. https://doi.org/10.1021/jp035057x
38. Milov AD, Tsvetkov YD, Formaggio F, Oancea S, Toniolo C, Raap J (2004) Solvent effect on the distance distribution between spin labels in aggregated spin labeled trichogin GA IV dimer peptides as studied by pulsed electron–electron double resonance. Phys Chem Chem Phys 6 (13):3596–3603. https://doi.org/10.1039/b313701e
39. Milov AD, Tsvetkov YD, Maryasov AG, Gobbo M, Prinzivalli C, De Zotti M, Formaggio F, Toniolo C (2013) Conformational properties of the spin-labeled tylopeptin B and heptaibin peptaibiotics based on PELDOR spectroscopy data. Appl Magn Reson 44(4):495–508. https://doi.org/10.1007/s00723-012-0402-1
40. Milov AD, Tsvetkov YD, Bortolus M, Maniero AL, Gobbo M, Toniolo C, Formaggio F (2014) Synthesis and conformational properties of a TOAC doubly spin-labeled analog of the medium-length, membrane active peptaibiotic ampullosporin A as revealed by CD, fluorescence, and EPR spectroscopies. Biopolymers 102(1):40–48. https://doi.org/10.1002/bip.22362
41. Rabenstein MD, Shin YK (1995) Determination of the distance between 2 spin labels attached to a macromolecule. Proc Natl Acad Sci USA 92(18):8239–8243. https://doi.org/10.1073/pnas.92.18.8239
42. Bortolus M, Tombolato F, Tessari I, Bisaglia M, Mammi S, Bubacco L, Ferrarini A, Maniero AL (2008) Broken helix in vesicle and micelle-bound alpha-synuclein: insights from site-directed spin labeling-EPR experiments and MD simulations. J Am Chem Soc 130 (21):6690–6691. https://doi.org/10.1021/jaB010429
43. Karle IL (1994) Diffraction studies of model and natural helical peptides. In: White SH (ed) Membrane protein structure: experimental approaches. Springer, New York, pp 355–380. https://doi.org/10.1007/978-1-4614-7515-6
44. Balashova TA, Shenkarev ZO, Tagaev AA, Ovchinnikova TV, Raap J, Arseniev AS (2000) NMR structure of the channel-former zervamicin IIB in isotropic solvents. FEBS Lett 466(2–3):333–336. https://doi.org/10.1016/S0014-5793(99)01707-X
45. Peggion C, Coin I, Toniolo C (2004) Total synthesis in solution of alamethicin F50/5 by an easily tunable segment condensation approach. Biopolymers 76(6):485–493. https://doi.org/10.1002/bip.20161
46. Crisma M, Peggion C, Baldini C, MacLean EJ, Vedovato N, Rispoli G, Toniolo C (2007) Crystal structure of a spin-labeled, channel-forming alamethicin analogue. Angew Chem Int Edit 46(12):2047–2050. https://doi.org/10.1002/anie.200604417

47. Milov AD, Tsvetkov YD, Formaggio F, Crisma M, Toniolo C, Raap J (2000) Self-assembling properties of membrane-modifying peptides studied by PELDOR and CW-ESR spectroscopies. J Am Chem Soc 122(16):3843–3848. https://doi.org/10.1021/ja993870t
48. Milov AD, Tsvetkov YD, Raap J (2000) Aggregation of trichogin analogs in weakly polar solvents: PELDOR and ESR studies. Appl Magn Reson 19(2):215–226. https://doi.org/10.1007/Bf03162276
49. Milov AD, Tsvetkov YD, Formaggio F, Crisma M, Toniolo C, Raap J (2003) Self-assembling and membrane modifying properties of a lipopeptaibol studied by CW-ESR and PELDOR spectroscopies. J Pept Sci 9(11–12):690–700. https://doi.org/10.1002/psc.513
50. Milov AD, Tsvetkov YD, Formaggio F, Crisma M, Toniolo C, Millhauser GL, Raap J (2001) Self-assembling properties of a membrane-modifying lipopeptaibol in weakly polar solvents, studied by CW ESR. J Phys Chem B 105(45):11206–11213. https://doi.org/10.1021/Jp011948y
51. Milov AD, Samoilova MI, Tsvetkov YD, Jost M, Peggion C, Formaggio F, Crisma M, Toniolo C, Handgraaf JW, Raap J (2007) Supramolecular structure of self-assembling alamethicin analog studied by ESR and PELDOR. Chem Biodivers 4(6):1275–1298. https://doi.org/10.1002/cbdv.200790110
52. Milov AD, Samoilova RI, Tsvetkov YD, Peggion C, Formaggio F, Toniolo C, Raap J (2006) Aggregation of spin-labeled alamethicin in low-polarity solutions as studied by PELDOR spectroscopy. Dokl Phys Chem 406:21–25. https://doi.org/10.1134/S0012501606010064
53. Marsh D (1989) Experimental methods in spin-label spectral analysis. In: Berliner LJ, Reuben J (eds) Spin labeling, theory and applications. Biological magnetic resonance, vol 8. Plenum Press, New York, pp 255–303. https://doi.org/10.1007/978-1-4613-0743-3
54. Stella L, Mazzuca C, Venanzi M, Palleschi A, Didone M, Formaggio F, Toniolo C, Pispisa B (2004) Aggregation and water-membrane partition as major determinants of the activity of the antibiotic peptide trichogin GA IV. Biophys J 86(2):936–945
55. Kropacheva TN, Raap J (2002) Ion transport across a phospholipid membrane mediated by the peptide trichogin GA IV. Biochim Biophys Acta (BBA)—Biomemb 1567:193–203. https://doi.org/10.1016/s0005-2736(02)00616-8
56. Milov AD, Samoilova RI, Tsvetkov YD, Formaggio F, Toniolo C, Raap J (2005) Membrane-peptide interaction studied by PELDOR and CW ESR: peptide conformations and cholesterol effect on the spatial peptide distribution in the membrane. Appl Magn Reson 29(4):703–716. https://doi.org/10.1007/Bf03166345
57. Salnikov ES, Erilov DA, Milov AD, Tsvetkov YD, Peggion C, Formaggio F, Toniolo C, Raap J, Dzuba SA (2006) Location and aggregation of the spin-labeled peptide trichogin GA IV in a phospholipid membrane as revealed by pulsed EPR. Biophys J 91(4):1532–1540. https://doi.org/10.1529/biophysj.105.075887
58. Milov AD, Erilov DA, Salnikov ES, Tsvetkov YD, Formaggio F, Toniolo C, Raap J (2005) Structure and spatial distribution of the spin-labelled lipopeptide trichogin GA IV in a phospholipid membrane studied by pulsed electron–electron double resonance (PELDOR). Phys Chem Chem Phys 7(8):1794–1799. https://doi.org/10.1039/b418414a
59. Milov AD, Samoilova RI, Tsvetkov YD, Formaggio F, Toniolo C, Raap J (2007) Self-aggregation of spin-labeled alamethicin in ePC vesicles studied by pulsed electron–electron double resonance. J Am Chem Soc 129(30):9260–9261. https://doi.org/10.1021/ja072851d
60. Bartucci R, Guzzi R, De Zotti M, Toniolo C, Sportelli L, Marsh D (2008) Backbone dynamics of alamethicin bound to lipid membranes: spin-echo electron paramagnetic resonance of TOAC-spin labels. Biophys J 94(7):2698–2705. https://doi.org/10.1529/biophysj.107.115287
61. Salnikov ES, De Zotti M, Formaggio F, Li X, Toniolo C, O'Neil JDJ, Raap J, Dzuba SA, Bechinger B (2009) Alamethicin topology in phospholipid membranes by oriented solid-state NMR and EPR spectroscopies: a comparison. J Phys Chem B 113(10):3034–3042. https://doi.org/10.1021/jp8101805

62. Milov AD, Samoilova RI, Tsvetkov YD, De Zotti M, Formaggio F, Toniolo C, Handgraaf JW, Raap J (2009) Structure of self-aggregated alamethicin in ePC membranes detected by pulsed electron–electron double resonance and electron spin echo envelope modulation spectroscopies. Biophys J 96(8):3197–3209. https://doi.org/10.1016/j.bpj.2009.01.026
63. North CL, BarrangerMathys M, Cafiso DS (1995) Membrane orientation of the N-terminal segment of alamethicin determined by solid-state N-15 NMR. Biophys J 69(6):2392–2397
64. Salnikov ES, Friedrich H, Li X, Bertani P, Reissmann S, Hertweck C, O'Neil JDJ, Raap J, Bechinger B (2009) Structure and alignment of the membrane-associated peptaibols ampullosporin A and alamethicin by oriented N-15 and P-31 solid-state NMR spectroscopy. Biophys J 96(1):86–100. https://doi.org/10.1529/biophysj.108.136242
65. Marsh D, Jost M, Peggion C, Toniolo C (2007) Lipid chain-length dependence for incorporation of alamethicin in membranes: electron paramagnetic resonance studies on TOAC-spin labeled analogs. Biophys J 92(11):4002–4011. https://doi.org/10.1529/biophysj.107.104026
66. Parsegian VA, Fuller N, Rand RP (1979) Measured work of deformation and repulsion of lecithin bilayers. Proc Natl Acad Sci USA 76(6):2750–2754. https://doi.org/10.1073/pnas.76.6.2750
67. Murzyn K, Rog T, Blicharski W, Dutka M, Pyka J, Szytula S, Froncisz W (2006) Influence of the disulfide bond configuration on the dynamics of the spin label attached to cytochrome *c*. Proteins-Struct Funct Bioinform 62(4):1088–1100. https://doi.org/10.1002/prot.20838
68. Spaar A, Munster C, Salditt T (2004) Conformation of peptides in lipid membranes studied by X-ray grazing incidence scattering. Biophys J 87(1):396–407. https://doi.org/10.1529/biophysj.104.040667
69. Reginsson GW, Schiemann O (2011) Studying bimolecular complexes with pulsed electron–electron double resonance spectroscopy. Biochem Soc T 39:128–139. https://doi.org/10.1042/Bst0390128
70. Goobes G, Stayton PS, Drobny GP (2007) Solid-state NMR studies of molecular recognition at protein-mineral interfaces. Prog Nucl Mag Res Sp 50(2–3):71–85. https://doi.org/10.1016/j.pnmrs.2006.11.002
71. Mirau PA, Naik RR, Gehring P (2011) Structure of peptides on metal oxide surfaces probed by NMR. J Am Chem Soc 133(45):18243–18248. https://doi.org/10.1021/ja205454t
72. Milov AD, Samoilova RI, Tsvetkov YD, Peggion C, Formaggio F, Toniolo C (2014) Peptides on the surface. PELDOR data for spin-labeled alamethicin F50/5 analogues on organic sorbent. J Phys Chem B 118(25):7085–7090. https://doi.org/10.1021/jp503691n
73. Syryamina VN, Samoilova RI, Tsvetkov YD, Ischenko AV, De Zotti M, Gobbo M, Toniolo C, Formaggio F, Dzuba SA (2016) Peptides on the surface: spin-label EPR and PELDOR study of adsorption of the antimicrobial peptides trichogin GA IV and ampullosporin A on the silica nanoparticles. Appl Magn Reson 47(3):309–320. https://doi.org/10.1007/s00723-015-0745-5
74. Banham JE, Baker CM, Ceola S, Day IJ, Grant GH, Groenen EJJ, Rodgers CT, Jeschke G, Timmel CR (2008) Distance measurements in the borderline region of applicability of CW EPR and DEER: a model study on a homologous series of spin-labelled peptides. J Magn Reson 191(2):202–218. https://doi.org/10.1016/j.jmr.2007.11.023
75. Stoller S, Sicoli G, Baranova TY, Bennati M, Diederichsen U (2011) TOPP: a novel nitroxide-labeled amino acid for EPR distance measurements. Angew Chem Int Edit 50 (41):9743–9746
76. Yang ZY, Kise D, Saxena S (2010) An approach towards the measurement of nanometer range distances based on Cu^{2+} ions and ESR. J Phys Chem B 114(18):6165–6174. https://doi.org/10.1021/jp911637s
77. Yang ZY, Ji M, Saxena S (2010) Practical aspects of copper ion-based double electron electron resonance distance measurements. Appl Magn Reson 39(4):487–500. https://doi.org/10.1007/s00723-010-0181-5

78. Maryasov AG, Tsvetkov YD, Raap J (1998) Weakly coupled radical pairs in solids: ELDOR in ESE structure studies. Appl Magn Reson 14(1):101–113. https://doi.org/10.1007/Bf03162010
79. Jun S, Becker JS, Yonkunas M, Coalson R, Saxena S (2006) Unfolding of alanine-based peptides using electron spin resonance distance measurements. Biochem US 45(38):11666–11673. https://doi.org/10.1021/bi061195b